Hindawi
Geofluids
Volume 2021, Article ID 7941989, 16 pages
https://doi.org/10.1155/2021/7941989

Research Article

Coupling Interaction of Surrounding Soil-Buried Pipeline and Additional Stress in Subsidence Soil

Yahong Ding,[1] Heng Yang,[1] Ping Xu,[1] Minxia Zhang,[1] and Zhenguo Hou[2]

[1]*School of Civil Engineering, Henan Polytechnic University, Jiaozuo, 454000 Henan, China*
[2]*China Construction Seventh Engineering Division Corp. Ltd., Zhengzhou, 450004 Henan, China*

Correspondence should be addressed to Ping Xu; xuping@hpu.edu.cn

Received 26 April 2021; Revised 11 June 2021; Accepted 7 August 2021; Published 25 August 2021

Academic Editor: Huie Chen

In the process of underground resource exploitation, the induced surface subsidence easily leads to the deformation and failure of buried pipeline. And in the process of soil subsidence, the complex interaction between buried pipeline and surrounding soil occurs, which leads to deformation and additional stress in buried pipeline. In this paper, a laboratory test system is designed and developed to analyze the influence of buried depth, cohesion of soil, and angle of internal friction on stress, in order to obtain the deformation mechanism of pipe-soil and the pressure around the pipe and the distribution of additional axial stress along the pipeline. The research results show that in the process of subsidence, the synergistic deformation between the pipe and soil at both ends of the subsidence area is maintained, while there is a compressive nonsynergistic deformation zone in the soil at the top of the pipe, and the deformation zone in the cohesion-less soil and the cohesive soil presents a spire shape and an arch shape, respectively. Areas of maximum additional tensile and compressive stresses occur in the area of maximum curvature and the central position. In addition, the smaller the burial depth, the earlier the unloading phenomenon occurs; and the additional stress in buried pipe in cohesion-less soil is significantly less than that in cohesive soil, and the unloading phenomenon occurs earlier. The research results provide the basis for disaster prevention of buried petroleum transmission pipeline in subsidence process.

1. Introduction

Today, most natural resources (e.g., petroleum, natural gas, oil, and water resources) are transported by buried pipelines, whose safety is central to ensuring the development of resources [1, 2]. However, due to underground resource extraction, groundwater pumping and underground engineering construction causes the upper soil to sink, forming an expansive sink curve, resulting in bending and deformation or damage to the buried pipelines [3, 4]. The interaction between the buried pipe and the soil around the pipeline is caused by the deformation of buried pipeline during soil subsidence and additional soil pressure around the pipeline [5, 6].

The study of the interaction between buried pipes and the soil around the pipes relies on indoor tests as well as numerical simulations. Tian et al. use a new formulation derived from the improved Spangler model to improve the accuracy of stress and deformation calculations for orthotropic buried pipes and demonstrate that the new model can simulate the behaviour of buried pipes better than the Spangler model [7]. Khademi-Zahedi uses the finite element method to evaluate the behaviour of buried medium density polyethylene (MDPE) pipelines where damage occurs at the crown. Buried gas pipelines are subjected to severe stresses during loading due to soil-structure interaction, the presence of traffic loads, the self-weight of the soil, daily or seasonal temperature variations, and uniform internal pressures [8]. Wu et al. use the orthogonal test method for sensitivity analysis of soil parameters and a comprehensive numerical study of the interaction between large diameter pipes and soils [9]. Wang et al. conduct a study of surface stress tests between room temperature or frozen sand and pipes to investigate the facial stress experienced by pipes buried in sand [10]. Zhang et al. develop a numerical simulation model of X80 pipeline under a reverse fault with a crossing angle of 60°,

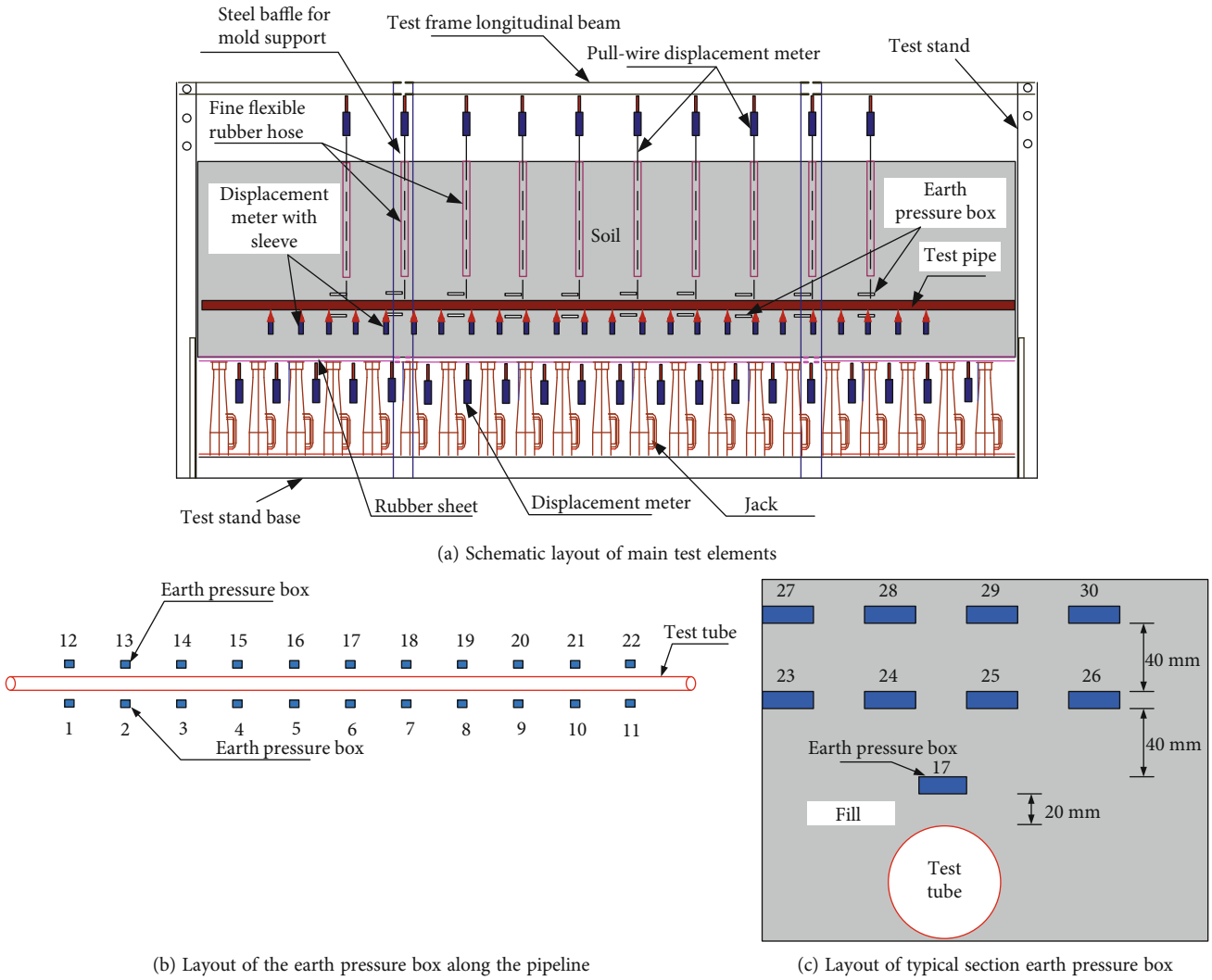

(a) Schematic layout of main test elements

(b) Layout of the earth pressure box along the pipeline

(c) Layout of typical section earth pressure box

Figure 1: Arrangement of the main test element.

analyze the damage evolution mechanism of buried steel pipeline, and discuss the effects of internal pressure and diameter-thickness ratio on the stress, strain, and displacement of the pipeline [11]. Bildik and Laman conduct an experimental study of stresses in buried pipes in cohesionless soils [12]. Zhou et al. use the experimental data to investigate the internal mechanistic behaviour and characteristics of surface subsidence in thick alluvial coal mining areas, which explains the peculiarities of surface subsidence in coal mining areas with thick alluvial layers and provides a basis for the establishment of predictive models [13].

The interaction during the relative movement of the pipe-soil is influenced by multiple parameters of the pipe-soil, which poses difficulties for indoor experimental studies, so it is of positive significance to analyze the influence of the pipe-soil parameters on the deformation and forces of buried pipes. Joneidi et al. consider the soil as an elastic material and derive its composition. The gas pipe is also modeled on a critical section below the road to study the axial stress as the maximum stress component and the displacement of the pipe [14]. Meidani et al. investigate the response of buried pipes under relative axial ground motion using three-dimensional discrete element analysis and develop a model for the continuous nature of the pipes. The microscopic parameters of the model are calibrated by triaxial tests [15]. Zhang et al. use a numerical simulation model to study the bending evolution mechanism of buried steel pipe under fault movement and discuss the influence of internal pressure of steel pipe, fault displacement, and diameter-thickness ratio of steel pipe on the bending of steel pipe [16]. Liu and Wang introduce the nonlinear pipe-soil interaction model into the analysis of lateral global bending of pipelines and investigate the bending characteristics of submarine pipelines with single-arch symmetric initial imperfections under different pipe-soil interaction models [17]. Ono et al. use fluid-coupled DEM (Discrete Element Method) to perform two-dimensional simulations of lateral loading experiments of pipes buried in saturated sand [18]. Weerasinghe et al. carry out an analysis of the moisture-controlled expansion/contraction behaviour of unsaturated soils based on finite element analysis software as an application of pipe stress analysis to quantify the stresses generated

(a) Displacement meter

(b) Displacement meter arrangement

(c) Multichannel data acquisition

Figure 2: Monitoring instruments and its arrangement for soil subsidence.

by reactive soil movements on pipes [19]. Monshizadeh Naeen and Seyedi Hosseininia investigate the deformation behaviour of buried steel pipes crossing active reverse faults by applying 3D continuous finite element modelling. Numerical simulations indicate that the local buckling (or wrinkling) failure mode is more sensitive to the pipe than the tensile failure mode [20]. The above indoor tests and numerical simulations mainly analyze the effect of soil resistance and deformation on buried pipes. However, the deformation and stress of the buried pipe is the result of the interaction between the pipe and the soil. To reveal the force and damage process of the buried pipe during subsidence, the distribution characteristics of the pipe-soil deformation and soil pressure during subsidence should be studied in depth.

In this study, a pipe-soil interaction test system is developed, and a corresponding numerical model study is carried out to determine the pipe-soil subsidence deformation, the top soil pressure, and the additional stress of the pipe during soil subsidence. Besides, in order to reveal the pipe-soil deformation mechanism during subsidence, the top deformation of the pipe and the distribution law of the additional axial stress along the pipe are analyzed, and the effect of pipe burial depth, soil cohesion, and internal friction angle on the additional soil pressure at the top of the pipe is obtained. The results provide a basis for analyzing the force characteristics of pipes in the subsidence area and establishing a mechanical analysis model for buried pipes during subsidence.

2. Laboratory Tests

2.1. Development of Test Systems. The experiment system is composed of test-bench system and test-test system (as shown in Figure 1(a)). The test bench is designed as a rectangular body with dimensions of 3200 mm (L) × 320 mm (W) × 2200 mm (H). The test bench base and vertical baffle are made of 32a channel steel cut and welded; the model bench support is made of no. 9 angle steel test bench base and vertical baffle welded; the cross-sectional size is 90 mm × 90 mm × 8 mm; the compression template is made of 2 pieces of steel template; the size is 310 mm × 1600 mm. In

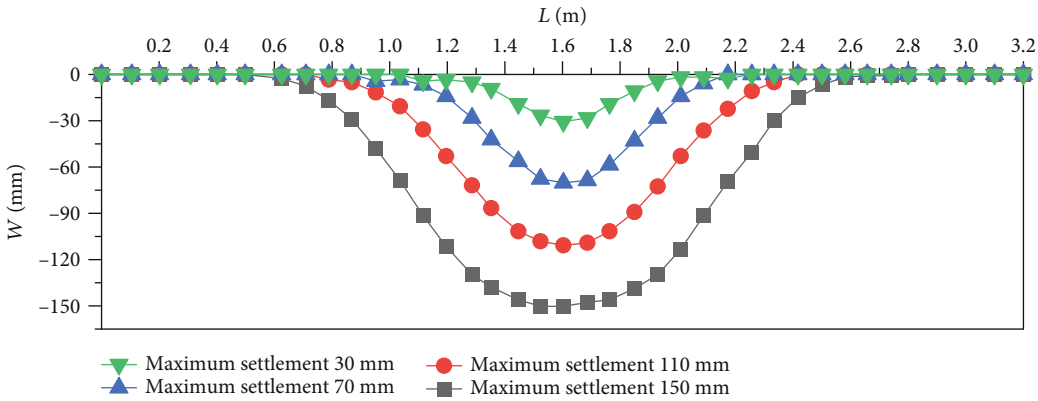

Figure 3: Test soil subsidence curve.

the test, the settlement of soil is controlled by Jack, the subsidence of soil is monitored by displacement meter arranged under Jack, and the settlement development process of soil along pipeline is realized. During the test, the jack was placed with the bottom of the soil and processed a steel cover plate on each jack of 320 mm × 125 mm, placed one transverse per 150 mm on the lower soil jack. Strain-gauge miniature earth pressure boxes are placed on the upper and lower sides of the pipe and on a typical section in the test, respectively, as shown in Figures 1(b) and 1(c), respectively, monitoring the evolution of the soil pressure around the pipe during soil subsidence using strain gauges. Real-time testing of test pipe subsidence values are used by a pull wire displacement meter. Real-time monitoring of relative pipe-soil deformation values are used by displacement gauges with sleeves [21, 22].

In order to control and monitor the subsidence volume of the soil, a displacement meter is arranged at the bottom of the steel cover, the maximum range of the displacement meter is 150 mm, and the measurement accuracy is 0.01 mm. The subsidence volume of each jack in each subsidence stage is calculated first during the subsidence of the soil, and the subsidence value is collected and monitored by the DM-201 multichannel data acquisition instrument produced by Hangzhou Xintec Technology Co. The displacement of the channel is shown in Figure 2.

The dimensions of the test bench are 3200 mm in length, 320 mm in width, and 2200 mm in height. The pipe is made of 50 mm diameter hard PVC material, which the size of the pipes and the range of soil affected by the interaction of the pipes and soil will be much smaller than the minimum size of the soil of the test bench (320 mm wide) to effectively avoid the influence of the size on the experimental results.

This experiment focuses on the soil-pipe interaction during subsidence. According to the deformation stiffness of the pipe and the characteristics of the soil, it was found by the preliminary test that when the pipe is buried at depth of 200~600 mm, the pipe and the soil will go through two stages of synergistic deformation and nonsynergistic deformation in the process of soil subsidence. Therefore, 400 mm pipe burial depth was used in this indoor laboratory. In order to further study the effect of soil burial depth on pipe soil interaction, the working conditions of 200 mm, 400 mm, and 600 mm pipe burial depth would be analyzed in numerical simulation. Based on the above test scheme design, the soil subsidence range and burial depth on the pipe soil interaction and pipe stress distribution characteristics will be analyzed in depth.

Figure 4: Observation of settlement of soil in pipeline layer.

2.2. Soil Subsidence Curve along Pipeline. The buried pipeline is an underground linear structure. When the subsidence range affects the buried pipeline, the subsidence of the buried pipeline becomes an expanded subsidence curve with the increase of the subsidence range. The subsidence range begins to affect the initial stage of buried pipeline, and the subsidence range and subsidence amount along the pipeline do not reach the maximum. With the expansion of the subsidence range, the subsidence range and subsidence amount of soil along the pipeline increases until the subsidence reaches the maximum. Based on the above deformation characteristics, the subsidence curve of the pipeline in this test adopts trigonometric function subsidence curve [23, 24], which is shown in Equation (1):

$$W(x) = W_m\left[n^2\left(1 - \frac{x}{D} + \frac{1}{2\pi}\sin 2\pi\frac{x}{D}\right) + \frac{1-n^2}{4}\left(1 + \cos\pi\frac{x}{D}\right)^2\right]. \quad (1)$$

$W(x)$ is the sink value at any point within the sink curve; W_m is the maximum sink value, taken as 30 mm, 70 mm,

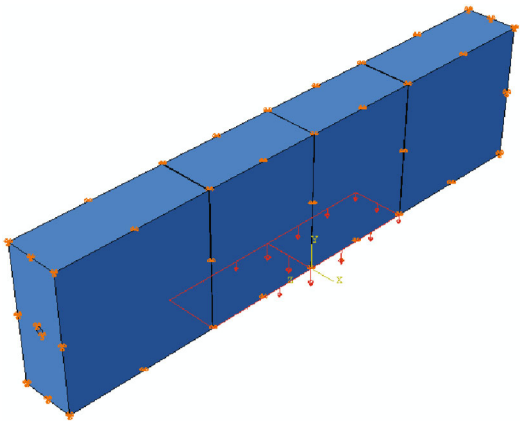

(a) Boundary constraints in the loading analysis step

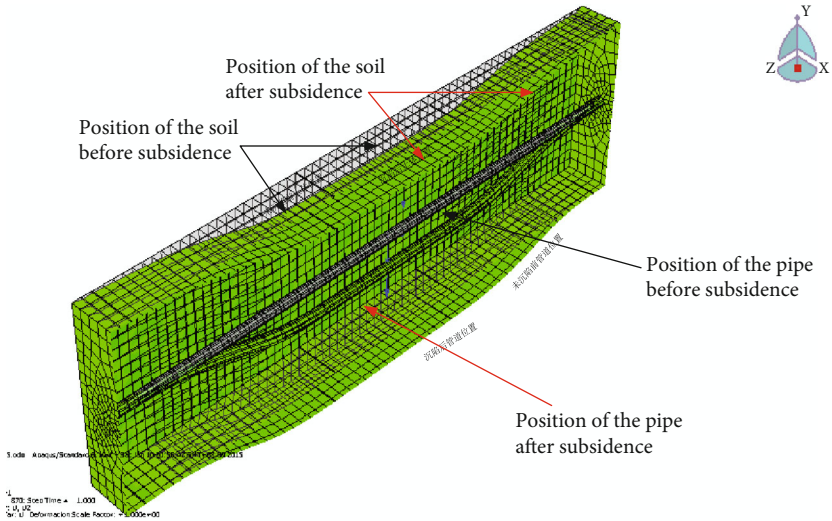

(b) Pipe-soil deformation after displacement load

Figure 5: Boundary conditions and loading of model.

110 mm, and 150 mm, respectively; n is the degree of subsidence factor, and the subsidence coefficient determines the shape of the subsidence curve, and the curvature at the bottom of the centre of the subsidence zone during subsidence changes from large to small; the larger the n, the smaller the curvature at the bottom of the centre of the subsidence zone. When $n = 1$, the bottom curvature of the subsidence area is zero (flat bottom), and the subsidence value reaches the maximum. In the test, n is taken as 0.25, 0.5, 0.75, and 1.0, respectively. The subsidence curve is symmetrical about the centre of the subsidence area, and D is the half of the length of the subsidence affected area along the pipeline. One end of the sunken soil in the indoor test is the origin, and the subsidence curves for each stage along the pipeline in the test are shown in Figure 3.

According to the evolution of the subsidence curve, the soil subsided in 4 steps (as shown in Figure 3). After each soil subsidence stabilizes, the settlement of pipeline soil is observed (as shown in Figure 4). At the end of the test, the soil is excavated, and the deformation and damage of the soil around the pipe are observed in a typical section.

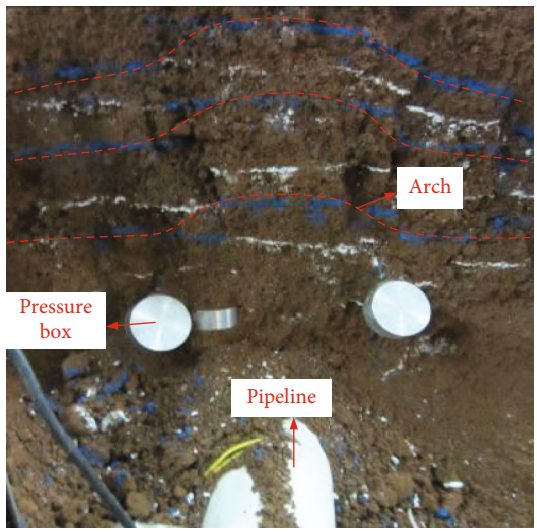

Figure 6: Deformation of soil on the upper side of pipe.

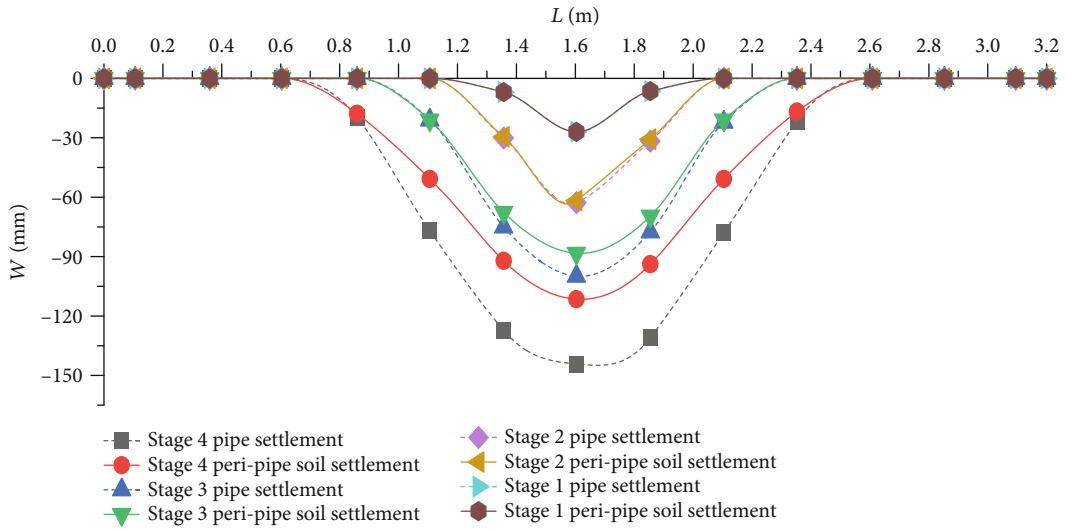

Figure 7: Deformation and evolution of pipe-soil during the development of collapse.

In the test, a hard PVC pipe with 50 mm diameter and 1.5 mm wall thickness, 35 MPa tensile strength, and 2.8 GPa tensile modulus is chosen. The test is arranged in the measurement point of the pull wire displacement meter, and the two ends of the pipe are fixed [25, 26]. The soil in the test is a cohesive soil with the cohesive force of 21 kPa and the internal friction angle of 30°. The cohesive force of sand is 0 kPa, and the angle of internal friction is 35. The density of clay is 1.718 g/cm^3, and the density of sand is 1.643 g/cm^3.

3. Numerical Simulation

During soil subsidence, the interaction between pipeline and soil around pipe is realized in ABAQUS numerical software [27, 28]. The behaviour of the pipe-soil contact introduces a contact surface unit and uses the master-slave contact surface to realize the pipe-soil interaction in the sunken soil. When the pipe-soil contact surface is in contact, the contact constraint is applied between the pipe-soil, and the contact pressure is transferred. When the contact pressure becomes zero, the pipe-soil contact surface is separated, and the contact constraint on the corresponding node is removed at the same time. In the setting of the master and slave surfaces of the contact surface, the wall surface with higher stiffness is chosen as the master surface and the surrounding soil as the slave surface. At the same time, the nodes on the side of the slave surface (pipe surrounding soil) is avoided to fall to the back of the master surface (pipe wall). At the time of meshing, the mesh on the slave side (pipe surrounding soil) is divided more finely than the main side (pipe wall). Contact surface transfers tangential stress (friction force), and Coulomb calculation of ultimate friction resistance is used in simulation [29].

The analysis step in numerical simulation is divided into initial analysis step and loading analysis step. In the initial analysis step, displacement constraints in the X, Y, and Z directions are applied to the sides of the model in the length direction, and displacement constraints in the Y direction are applied to the bottom, and displacement constraints in the X and Y directions are applied to both ends of the pipe. In the loading analysis step, the displacement constraints in the Y direction of the subsidence range are lifted, and the subsidence curve from the indoor test is used to load the displacement of the soil along the subsidence range of the pipe, as shown in Figure 5(a), and the displacement loading function is in Equation (1). After displacement loading, the soil in the pipeline and subsidence area sinks. The pipe-soil deformation after applying displacement load is shown in Figure 5(b).

In order to analyze the influence of soil around the subsidence pipe on the mechanical response of buried pipeline, the effects of different burial depths, different soil qualities, and different friction angles within the soil on the mechanical response of buried pipes are simulated and analyzed. The numerical models with buried depth of 200 mm, 400 mm, and 600 mm are established, and the influence of different buried depth and soil parameters on the additional stress of pipeline is analyzed.

4. Results and Analysis

4.1. Deformation Characteristics of Pipe-Soil during Subsidence

4.1.1. Pipe-Soil Congruence during Subsidence. In the laboratory test, the soil subsidence is divided into four stages. In order to reflect the synergistic relationship between pipeline and soil around the pipe in real time, the subsidence value of pipeline in each subsidence stage is compared with the subsidence monitoring value of soil in the same layer of pipeline (as shown in Figure 6). The solid line is the settlement curve of the pipeline, and the dashed line is the settlement curve of the soil of the same layer of the pipeline.

It is obvious that the subsidence value and subsidence curve of buried pipeline in the first and second subsidence

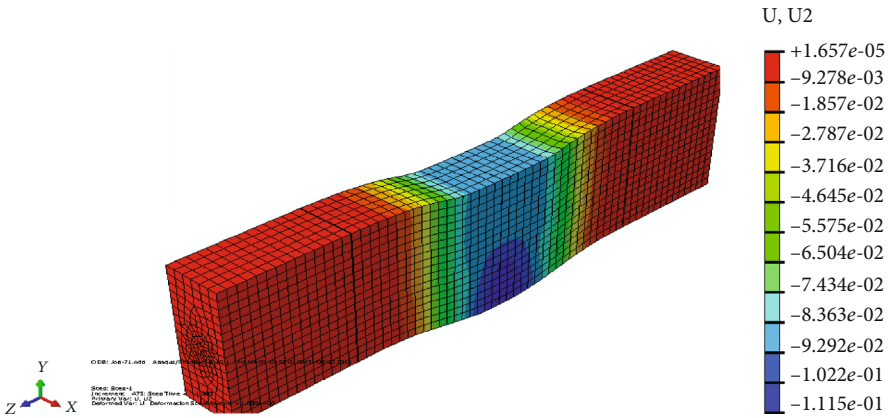

Figure 8: Clouds of soil deformation along pipeline.

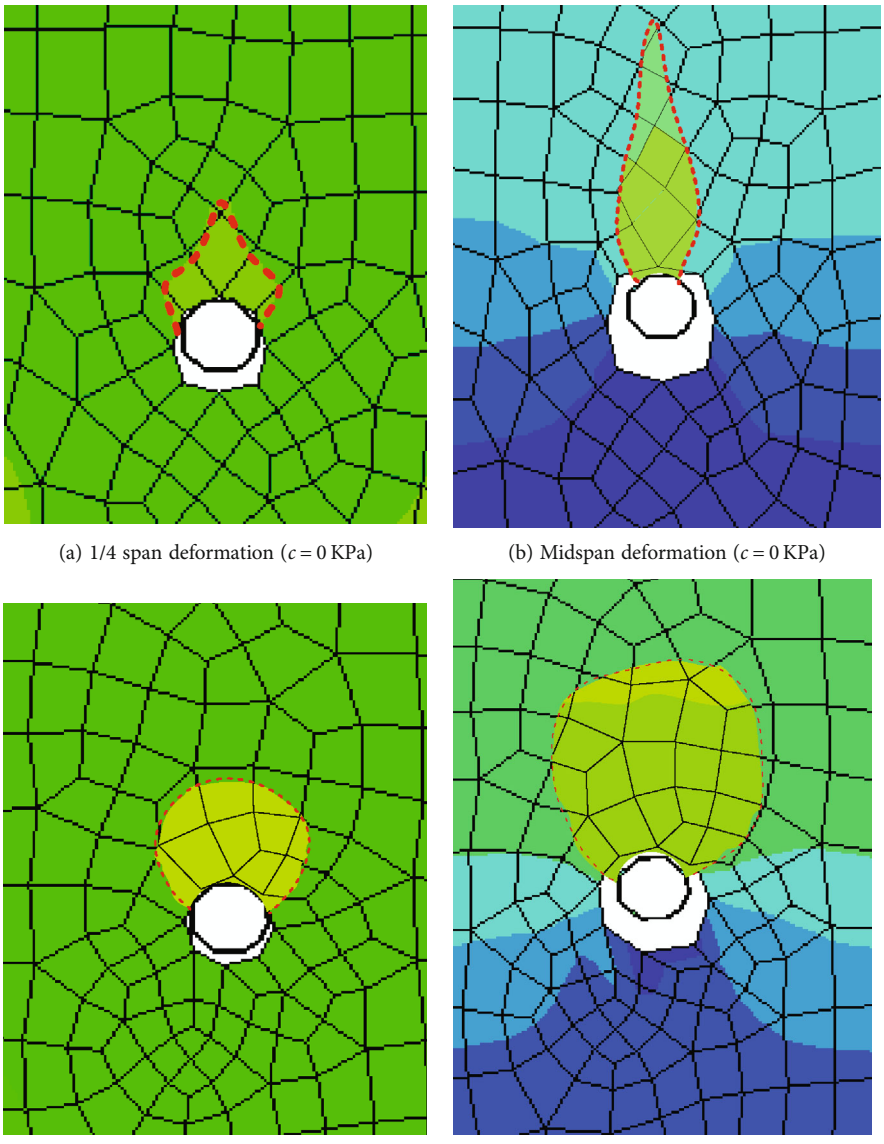

(a) 1/4 span deformation ($c = 0$ KPa)

(b) Midspan deformation ($c = 0$ KPa)

(c) 1/4 span deformation ($c = 20$ KPa)

(d) Midspan deformation ($c = 20$ KPa)

Figure 9: Deformation of soil in pipeline section.

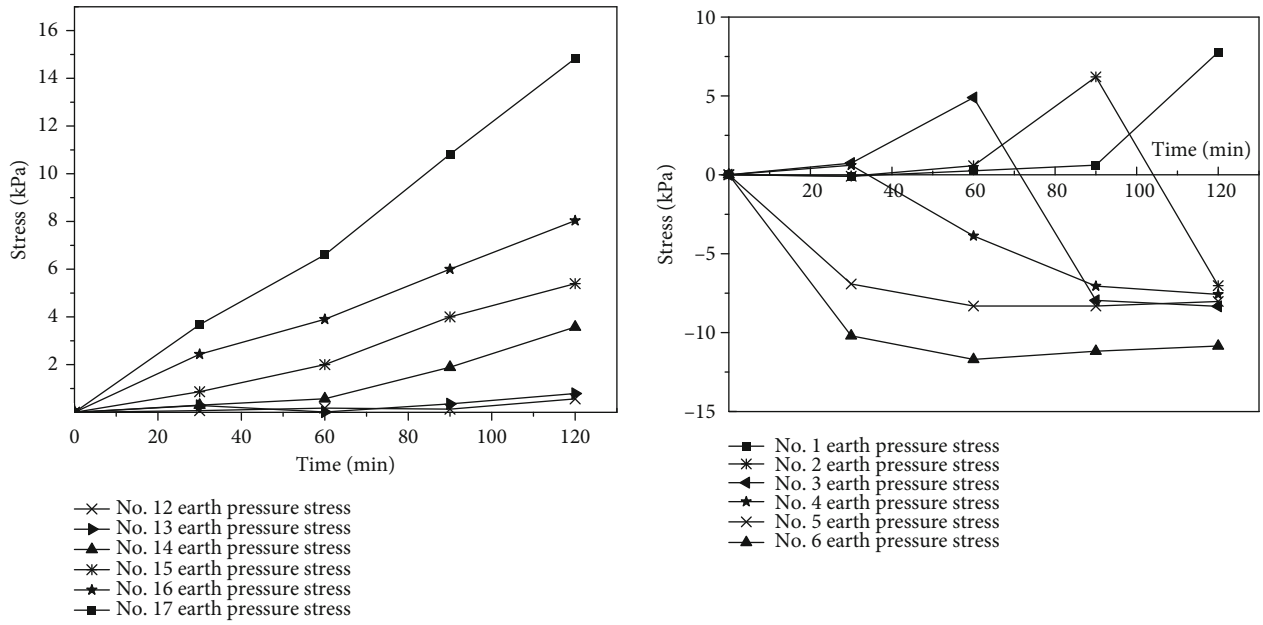

(a) The process of pressure evolution on the upper side of the pipeline

(b) The evolution process of the lateral earth pressure under the pipeline

Figure 10: Evolution of soil pressure along pipeline.

stages are basically consistent with the soil around the pipe, namely, the pipeline and the soil around the pipe are synergistic subsidence deformation in the initial subsidence stage. The mechanical response of buried pipeline is analyzed. After the third subsidence stage, the subsidence value of the soil in the middle of the pipe is greater than the subsidence value of the pipe, nonsynergistic deformation of the pipe, and the surrounding soil, but the surrounding soil and the pipe remain synergistic at both ends of the subsidence curve. With the increase of the soil subsidence range and subsidence value, the nonsynergistic deformation range of the pipe and the soil around the pipe gradually increases, and the maximum value of the pipe-soil settlement difference appears near the maximum curvature of the soil subsidence curve in the middle of the subsidence area. When the pipe line and the soil around the pipe produce nonsynergistic subsidence, the pipeline is divided into a pipe-soil synergistic deformation zone and a nonsynergistic deformation zone, and the subsidence value of the soil along the pipe line is regarded as the subsidence deflection of the pipe. In the zone of nonsynergistic pipe-soil deformation, an analytical model is developed based on the distribution of additional earth pressures along the pipeline.

4.1.2. Characteristics of Soil Deformation at the Top of the Pipe. In order to analyze the deformation and failure characteristics of the soil at the top of the pipeline during the settlement of the soil, the marking surface is arranged in the top soil of the 1/4 span and the middle span of the pipeline in the laboratory test. The deformation of soil around the pipe on the typical 1/4 cross section is shown in Figure 7. In Figure 6, the upper part of the soil near the pipe shows a misshapen fracture surface, the maximum dislocation distance is about 25 mm, and the maximum dislocation momentum decreases from bottom to top. At the top of the pipe about 110 mm, the soil begins to appear arc compression surface. The expansion angle is about 75 degrees. The compression deformation range is limited to a certain height of soil at the top of the pipeline, namely, there is an equal subsidence surface in the upper soil layer of the pipeline.

The binding force on the top of the pipe is closely related to the compression deformation and shape of the top soil. The deformation of soil on the upper side of the pipe in the third subsidence stage is analyzed below. The cloud diagram of soil deformation along the pipeline is shown in Figure 8. The Figure 8 shows the overall soil settlement; because of the difference of the stiffness between the soil and the pipe, there will be nonsynergistic deformation in the settlement process, thus creating a soil arch area generated inside the soil body, corresponds to that shown in Figure 6. The numerical legend in the figure shows the displacement deformation values.

During settlement, there are pipe-soil synergistic deformation zone and nonsynergistic deformation zone, due to different deformation stiffness of soil and pipeline in Figure 8. As the settlement proceeds, the lower soil of the pipe is separated from the pipe to create a gap area. Figures 9(a) and 9(b) show the tip-shaped area generated at the top of the pipe without cohesive soil, because there is no bonding force in the cohesive soil, so no large additional stress is generated. Figures 9(c) and 9(d) show the deformation area generated at the top of the pipe with cohesive soil as a circular arc-shaped area with a continuous arc at the top of the area. Such a result is due to the internal bonding force of the clayey soil. The blank area below the pipe in Figure 9 is the result of the separation of pipe and soil. When the pipe-soil settles, the soil below the pipe settles faster than the pipe settles, producing a pipe-soil gap area.

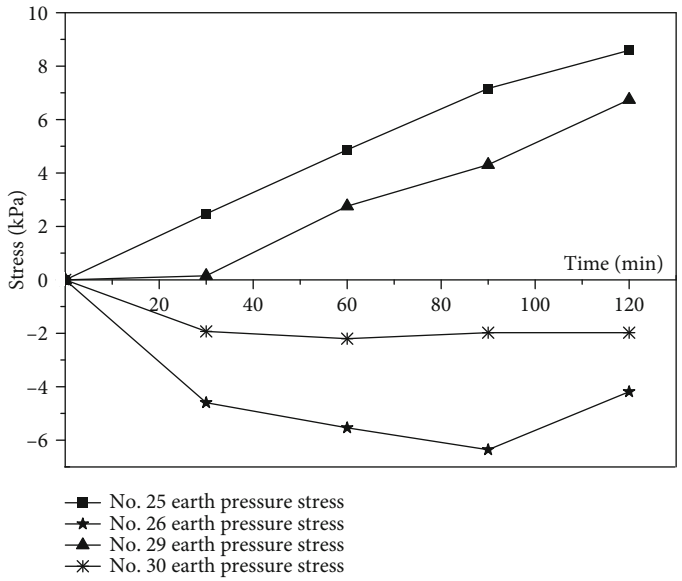

Figure 11: Typical section soil pressure evolution.

Two sections are intercepted in 1/4 span and middle span of subsidence area. The soil deformation of pipeline section when soil cohesion $c = 0$ kPa (cohesion-less soil) is shown in Figures 9(a) and 9(b), and the soil deformation of pipeline section when $c = 20$ KPa is shown in Figures 9(c) and 9(d). The results show that the pipe-soil nonsynergistic subsidence occurs on the lower side of the pipe in 1/4 span and middle span of the subsidence area, when the deformation of the upper side of the pipe and the surrounding soil have nonsynergistic deformation dotted line mark in Figure 9, and the subsidence value of the upper side of the pipe is obviously smaller than that of the surrounding soil. When the cohesive force $c = 0$ KPa (cohesion-less soil), the nonsynergistic deformation zone of the soil on the upper side of the pipe shows a cusp topping pattern; at cohesion $c = 20$ KPa, the nonsynergistic deformation zone of the soil on the upper side of the pipe shows an arch shape. The nonsynergistic pipe-soil subsidence values and deformation zones are larger on the transverse interruption surface; at cohesion $c = 0$ KPa, the cusp of the nonsynergistic deformation zone at the top of the pipe develops rapidly upwards; while at a cohesion $c = 20$ KPa, the nonsynergistic deformation zone at the top of the pipe expands simultaneously to the sides and the top. By analyzing the morphology and characteristics of the nonsynergistic deformation zone of the soil on the upper side of the pipe, the area of the nonsynergistic deformation zone at the top of the pipe is smaller in soils with cohesion $c = 0$ KPa than in soils with $c = 20$ KPa, and the tip of the nonsynergistic deformation zone of the pipe-soil develops rapidly upwards, and a vertical single shear surface is formed in the soil, which is the main reason for the smaller binding force at the top of its pipe. The use of cohesion-less soils for buried pipes is beneficial for reducing the additional stresses in buried pipes during subsidence.

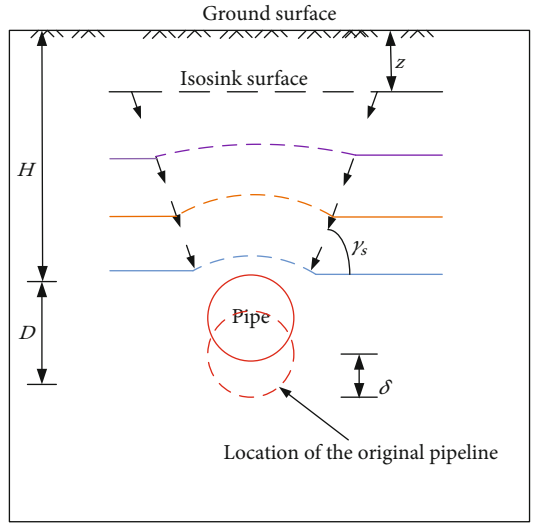

Figure 12: Compression of the soil at the top of pipeline in subsidence soil.

4.2. Characteristics of the Distribution of Pressure around the Pipe in the Subsidence Soil. During the indoor test, the soil pressure is collected at 30 min, 60 min, 90 min, and 120 min. In the process of collecting earth pressure, the pressure is first balanced. That is, the data collected by earth pressure box are additional stress. The arrangement position of the upper and lower side earth pressure boxes of the pipeline is symmetrical about the no. 17 and no. 6 earth pressure boxes, respectively. The distribution of the earth pressure at the left end of the pipeline is analyzed. The strain evolution process of 12~17 and 1~6 earth pressure boxes on the upper side of the pipeline during soil subsidence is shown in Figure 10.

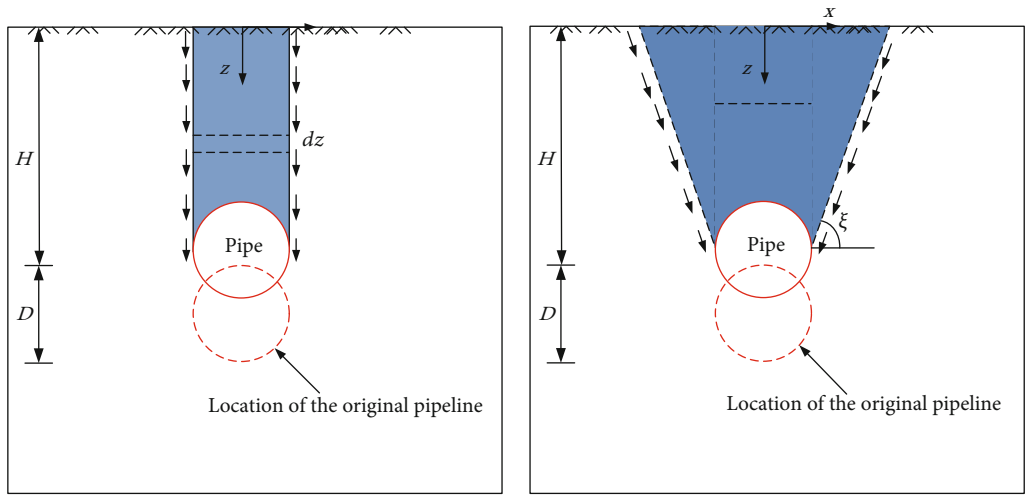

(a) Top soil column of pipe in cohesion-less soil (b) Top soil column of pipe in cohesive soil

Figure 13: Shear plane in sol column at the top of pipeline.

Additional earth pressure is collected along the upper side of the pipeline in Figure 10(a). The additional soil pressure increases with the increase of soil settlement in stages 1 and 2. Because the soil at the bottom of the pipe produces more subsidence deformation than the pipe deformation, the support function of the soil around the pipe is weakened, and the additional stress on the upper side of the pipe mainly comes from the weight of the soil shared by the top of the pipe; in stages 3 and 4 (90 min and 120 min), the subsidence value of the pipe is less than that of the soil around the pipe. The pipe begins to compress the upper soil, and the pressure growth rate of the upper side of the pipeline increases. As the subsidence area expands, the lower side of the pipeline forms an unloading area. During the second subsidence phase (60 min), unloading occurs at no. 4 to no. 6. But there is an obvious pressurization at no. 3; pressurization also occurs at the lower side of the pipe at the edge of the subsidence area in the third and fourth subsidence stages (90 min and 120 min). This shows that during the subsidence, the bottom of the pipe is not all areas of pressure unloading; at the end of the edge of the subsidence zone, the bottom of the pipe is pressurized. The main reason for this phenomenon is that during soil subsidence, the soil on the upper side of the pipe exerts downward earth pressure on the pipe; the subsidence velocity of the soil in the lower part of the pipeline in the subsidence area is greater than that of the pipeline. At this point, the pipe support pressure shifts to both ends of the edge of the subsidence area. There is an increase in support force on the lower side of the edge pipeline in the subsidence area, causing the increase of earth pressure. In Figure 10(b), 0~30 min stage is the first stage of settlement; the middle of the pipe (positions 5 and 6) will be the first to deform to produce unloading effect, so the curve in the figure produces negative pressure; then, in the second stage, it is obvious to see that no. 3 has positive pressure value, because the pipe support pressure will be transferred to the two ends of the edge of the subsidence area, so it produces an increase of the support force on the lower side of the edge pipe, which is shown in the figure as positive pressure curve. The mutation points in the curves are the same as this principle.

In order to analyze the change of soil pressure in the soil layer at the top of the pipeline, the soil pressure box is arranged in the typical section in the middle of the pipeline to test the change of soil pressure in the upper soil of the pipeline during subsidence (as shown in Figure 10(a)). The earth pressure evolution pattern of the earth pressure box at the right-hand position of a typical section (positions no. 25, no. 26, no. 29, and no. 30) is analyzed, and the strain evolution process is shown in Figure 11.

The earth pressure box at position 25 begins to appear additional earth pressure in the first subsidence stage (30 min), and the upper 29 earth pressure is zero, namely, the additional earth pressure decreases gradually from the top of the pipe. According to Figure 11, we can also see that no. 25 and no. 29 produce essentially the same degree of change in the four settling stages, without excessive differences between the several stages. In the course of subsidence, pressure unloading occurs in the no. 26 and no. 30 positions, caused by the compression arch in the upper part of no. 26 and no. 30. From the strain evolution of soil pressure in a typical section, it can be inferred that the compressed soil at the top of the pipe in soil subsidence expands from the top side of the pipe to both sides, generating a pressurizing effect within the compressed soil. At the same time, it can be seen that the unloading states no. 26 and no. 30 out of the pressure state tend to increase gently, except in the first stage after the first unloading phenomenon in the second three or four stages did not produce too much change.

4.3. Pressure of Soil at the Top of Pipe in Subsidence Soil. In the process of soil subsidence, the soil pressure of buried pipeline includes initial soil pressure and additional soil pressure. The initial soil pressure is caused by the weight of the soil around the pipe, and the additional soil pressure is caused by the pipe-soil interaction in the subsidence soil.

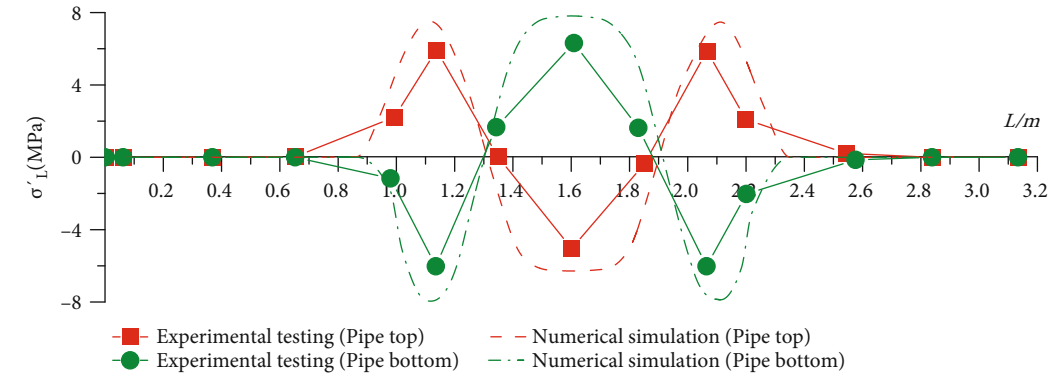

(a) Stress distribution at the top and bottom of the pipe during subsidence stage 1

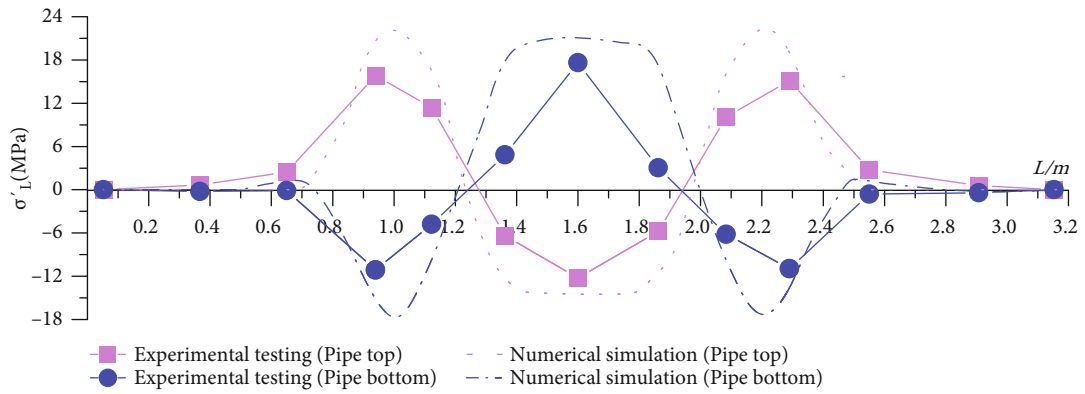

(b) Stress distribution at the top and bottom of the pipe during subsidence stage 2

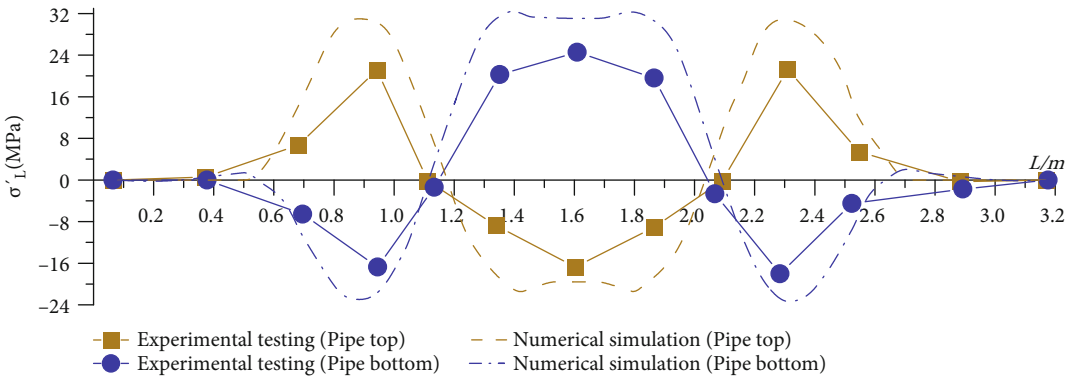

(c) Stress distribution at the top and bottom of the pipe during subsidence stage 3

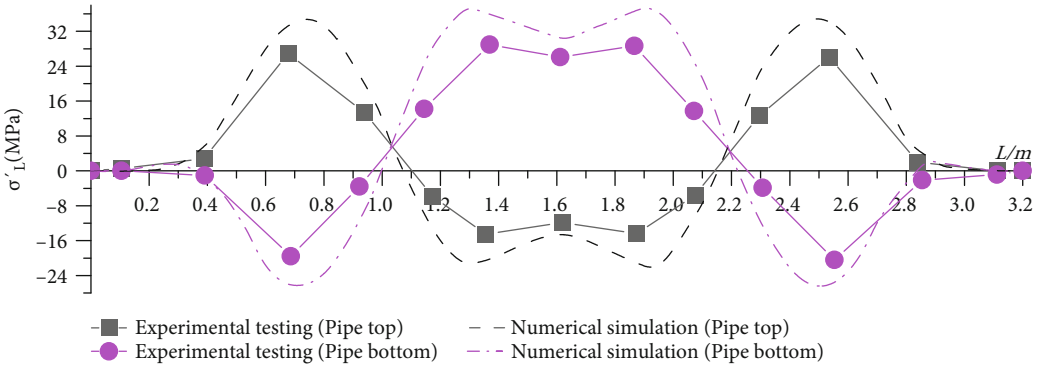

(d) Stress distribution at the top and bottom of the pipe during subsidence stage 4

Figure 14: Distribution of axial stress at top and bottom of pipe.

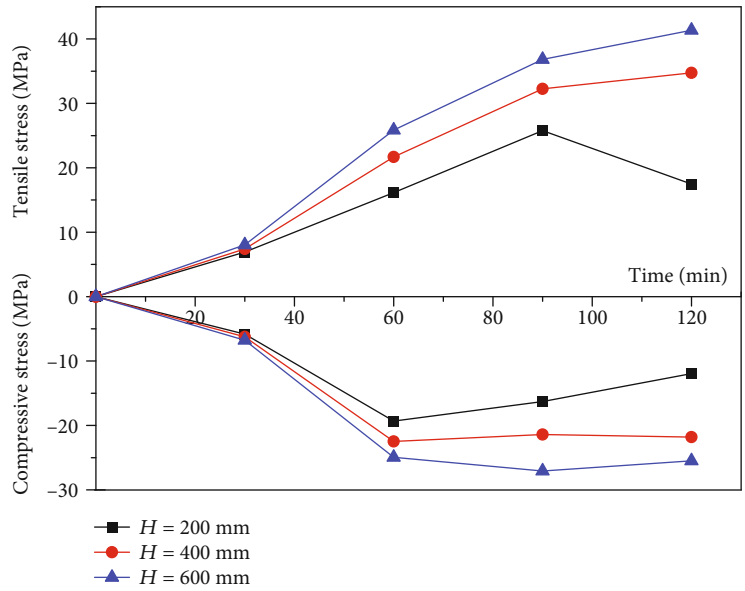

Figure 15: Maximum additional axial stress of pipelines under different buried depths.

In the process of soil subsidence, the soil pressure on both sides of the pipeline is considered to be approximately equal, and the additional soil pressure of the pipeline considers the top soil pressure of the pipe. The soil pressure at the top of the additional pipe increases with the increase of the relative deformation between the pipe and the soil until the limit value is reached, when the soil at the top of the pipe is shearing.

Because the subsidence velocity of the pipeline is smaller than that in the surface, the settlement of the soil column on the upper side of the pipe is less than that of the soil column outside the pipe, and the settlement difference is δ. This compression deformation is limited to a certain height H_s on the upper side of the pipe. There is an equal settlement surface in the upper soil layer of the pipe, and the height of the equal sinker from the top of the pipe is H_s. As shown in Figure 12, H_s gradually increases with the increasing ground deformation along the pipeline route; when $H_s = H$, the surface soil at the location of the corresponding pipe arches upwards, and the soil on the upper side of the pipe is damaged, and the additional earth pressure at the top of the pipe reaches its limit. When $H_s < H$, considering the additional earth pressure in the upper part of the pipe as a uniform load $\Delta\sigma$, the above problem is transformed into a problem of compressive deformation of the soil under the action of a uniform load in the form of a strip. The soil is regarded as a semi-infinite elastic medium with $\Delta\sigma$ uniform load. According to the elastic theory, the corresponding calculation formula of the $\Delta\sigma$ of settlement difference δ can be obtained as follows [30]:

$$\Delta\sigma = \frac{\delta E_s}{L\omega_c(1-\mu^2)}. \tag{2}$$

E_s is the deformation modulus of soil, and μ is the Poisson ratio of fill on the upper side of the pipe, and ω_c is the calculated aspect ratio (L'/D) of rigid pipeline, and L' is the calculated length of load.

When $H_s = H$, the height of the equal sink surface reaches the ground surface, and the ground surface soil gradually arches upwards and gradually forms a through shear surface, and the additional earth pressure at the top of the pipe reaches its limit. The top soil pressure includes the soil weight on the upper side of the pipe and the shear stress on the shear surface. In the process of soil subsidence, the shear surface of the top soil varies with the soil quality. According to the test results, when the upper side of the pipe is clay, the shear section is regarded as a straight line, and the shear section of the soil on the upper side of the pipe extends to both sides of the top of the pipe. The angle between the shear section and the pipeline plane is ξ (as shown in Figure 13(b)).

For cohesion-less soil, when calculating the pressure of the limit pipe top soil in the subsidence soil, the influence of soil cohesion is not taken into account. The vertical resistance of the pipe top per unit length of buried pipeline along the pipeline q_{v1} is a function of shear surface friction and soil weight on the upper side of the pipe. As shown in Figure 13(a), the equation is as follows:

$$q_{v1} = \gamma HD + 2\int_0^H K\gamma \tan\phi dz = \gamma HD + K\gamma H^2 an\phi, \tag{3}$$

γ is heavy soil, N/m^3; $\varnothing$ is internal friction angle.

For cohesive soils, the vertical surrounding soil pressure q_{v2} at the top of the pipe per unit length of buried pipes along the pipeline not only takes the self-weight of the soil overlying the pipe into account but also takes the combined effect of cohesive soil cohesion and internal friction angle into account, as shown in Figure 13(b), for the buried pipeline along the pipeline. The effect of cohesive force and

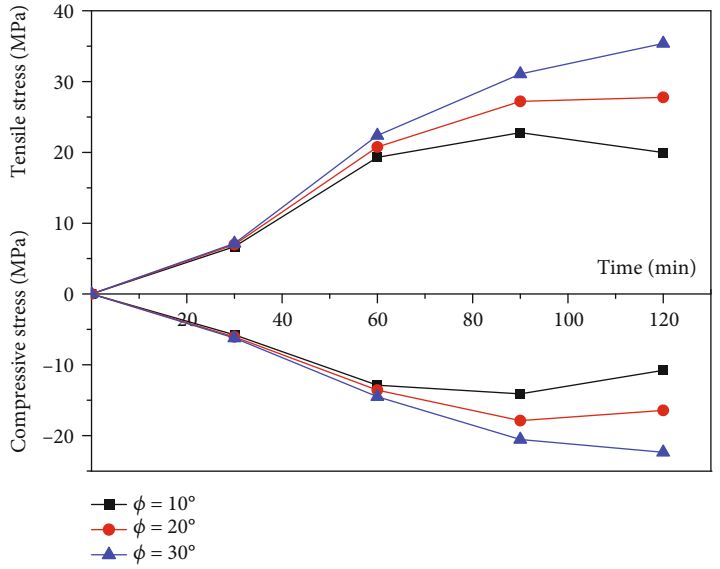

(a) Additional axial stress at the top of the pipe under the influence of internal friction angle ($c = 20$ kPa)

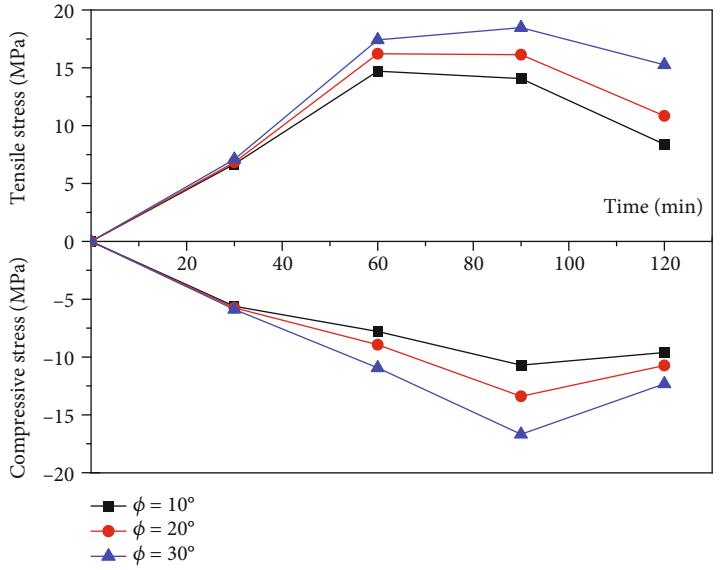

(b) Additional axial stress at the top of the pipe under the influence of internal friction angle ($c = 0$ kPa)

Figure 16: Influence of soil parameters on additional axial stress in pipes.

internal friction angle on the soil pressure around the vertical pipe is reflected by undrained shear strength C_u. The equation are as follows:

$$q_{v2} = \gamma\left(\frac{(HD + H^2)}{\tan \xi}\right) + \frac{2C_u H}{\sin \xi}, \tag{4}$$

C_u is the undrained shear strength of soil.

4.4. Additional Axial Stress in Piping during Subsidence

4.4.1. Characteristics of Axial Stress Distribution in Pipeline. For the characteristics of additional axial stress distribution, strain gauges are arranged along the pipeline in the test, and the corresponding numerical simulation analysis is carried out at the same time. The axial stress distribution along the top and bottom of the pipeline numerically simulated and tested during subsidence is shown in Figure 14.

As shown in Figure 14. In each subsidence stage, there are both tension zone and compression zone along the bottom and top of the pipeline. In the first subsidence stage, the tensile and compressive stresses on the top and bottom of the pipe are basically equal, because the subsidence range is small, and the axial friction resistance of the soil along the pipeline is small, which is mainly affected by bending stress. With the expansion of the subsidence area, the axial friction of the soil along the pipeline increases gradually. Because the axial deformation of the soil around the pipe in the subsidence area is larger than the tensile deformation

of the pipe, the friction force of the soil in the subsidence area is mainly tensile stress, causing the additional tensile stresses in the cross-section of the pipe in the sinkhole to be greater than the additional compressive stresses. When the extent of subsidence has progressed to stage 4 of subsidence, a large additional axial stress is generated at the position of maximum curvature and at the center of the subsidence zone. The reason is that although the center of the subsidence area is not the location of the maximum curvature of the pipe deformation, but which is subjected to a larger pipe-soil friction axial force (tensile stress) and bending axial stress, the axial tensile stress is larger. Combined with the soil subsidence curve along the pipeline, the maximum additional tension and compressive stress zone of the pipeline are located at the center of the maximum curvature and subsidence zone, where the pipeline is prone to yield. The distribution law of additional axial stress in each subsidence stage in numerical simulation is basically the same as the test results.

4.4.2. Influence of Buried Depth and Soil Parameters on Additional Axial Stress of Pipeline. To analyze the influence of buried depth on the additional axial stress of pipeline, the maximum additional tensile stress and compressive stress along the pipeline with buried depth of 200 mm, 400 mm, and 600 mm are analyzed, respectively. As shown in Figure 15, the tensile stress is positive, and the compressive stress is negative. In the initial stage of subsidence (0~30 min), the additional stress of pipeline under different buried depth is almost the same, and with the development of subsidence, the influence of buried depth on the additional stress of pipeline is obvious. The larger the buried depth, the more obvious the soil at the top of the pipeline is, the greater the additional axial stress, and the smaller the buried depth; the binding force of the soil on the top of the pipeline reaches the limit first, resulting in an unloading phenomenon. Therefore, reducing the burial depth of the pipeline in the subsidence area is beneficial for reducing the additional axial stress along the pipeline.

The influence of the cohesion of the soil around the pipe and the angle of internal friction on the additional axial stresses along the pipe during the development of subsidence is analyzed. Maximum additional tensile and compressive stresses along in the pipe surrounding soil with different internal friction angles of 0 and 20 kPa at a burial depth of 400 mm are analyzed, respectively (as shown in Figure 16).

When the soil subsidence along the pipeline is small, the influence of soil cohesion and internal friction angle on the additional stress of the pipeline is relatively small, and the influence is gradually obvious with the increase of subsidence range. Reducing soil cohesion and internal friction angle is beneficial for reducing the additional axial stress of buried pipeline in subsidence area. The additional stress of buried pipeline in cohesion-less soil ($c = 0$ kPa) is obviously smaller than cohesive soil, and the unloading phenomenon of buried pipeline in cohesion-less soil occurs earlier. Therefore, the sand buried pipeline with less cohesive force is more conducive to reducing the additional axial stress along the pipeline during subsidence.

5. Conclusions

Based on the developed laboratory test and numerical simulation, the deformation characteristics of buried pipe-soil during the development of subsidence, the soil pressure around the pipe, and the additional stresses along the pipe are determined, and the distribution laws of pipe-soil deformation, soil pressure around the pipe, and additional stresses along the pipe are obtained. The main conclusions are as follows:

(1) During the subsidence of the soil along the pipe, the pipe and the soil around the pipe undergoes synergistic and nonsynergistic subsidence deformation. In the area of synergistic deformation of the pipe and soil, the subsidence value of the soil along the pipe is regarded as the subsidence deflection of the pipe, building a mechanical analysis model of the pipe; while in the area of nonsynergistic deformation of the pipe and soil, the analysis model needs to be built, according to the distribution law of the additional earth pressure along the pipe

(2) In the process of subsidence, there is a compressed nonsynergistic deformation zone in the soil at a certain height at the top of the pipe. The deformation zone in the cohesion-less soil shows a cusp shape, and a vertical single shear surface is formed in the soil; the cohesive soil shows an arch shape, and the compressed soil expands from the upper side of the pipe to both sides, and the compressed soil produces a pressure increase within the compressed soil. The additional soil pressure at the top of the pipe increases as the soil settles, and an unloading zone is formed locally on the lower side, with the soil pressure shifting towards the edge of the sinkhole and the phenomenon of increased pressure

(3) In the process of subsidence, the pipe is subjected to the combined action of bending and the axial friction of the pipe and soil, and the maximum additional tension and compressive stress zone is located in the maximum curvature and central position of the subsidence zone, where the pipe is prone to yield. In the process of subsidence development, the smaller the buried depth, the more the binding force on the pipeline reaching the limit; thus, the unloading phenomenon occurs, and the additional stress of the buried pipeline in the cohesion-less soil is obviously smaller than the cohesive soil, and the unloading phenomenon appears earlier. Therefore, reducing the buried depth of the pipeline in the subsidence area and adopting the sand buried pipeline with less cohesion are beneficial for reducing the additional axial stress along the pipeline

Data Availability

The data used to support the findings of this study are included within the article.

Conflicts of Interest

The authors declare that they have no conflicts of interest.

Acknowledgments

Financial supports from the Key Science and Technology Program of Henan Province, China (No. 202102310253), the Youth Key Teacher Project of Henan Provincial Colleges and Universities (2017GGJS054), Joint Funds of the National Natural Science Foundation of China (No. U1904188), the Doctor Foundation of Henan Polytechnic University (No. B2016-67), and the Science and Technology Project of Henan Provincial Department of Transportation, China (No. 2019J-2-13) are gratefully appreciated.

References

[1] C. Z. Liu and Y. H. Su, "Pipeline deformation laws and safety risk assessments caused by shield construction," *Journal of Railway Science and Engineering*, vol. 17, no. 11, pp. 2882–2891, 2020.

[2] L. Zhu, F. Dang, Y. Xue, K. Jiao, and W. Ding, "Multivariate analysis of effects of microencapsulated phase change materials on mechanical behaviors in light-weight aggregate concrete," *Journal of Building Engineering*, vol. 42, article 102783, 2021.

[3] P. Liu, Y. X. Li, Y. Zhang, M. Y. Sun, Y. Zhang, and Y. Zhang, "Stress calculation of buried pipelines affected by typical geological hazards," *Oil & Gas Storage and Transportation*, vol. 40, no. 2, pp. 157–165, 2021.

[4] Y. Xue, J. Liu, P. G. Ranjith, X. Liang, and S. Wang, "Investigation of the influence of gas fracturing on fracturing characteristics of coal mass and gas extraction efficiency based on a multi-physical field model," *Journal of Petroleum Science and Engineering*, vol. 206, article 109018, 2021.

[5] Z. Cao, Y. Ren, Q. Wang, B. Yao, and X. Zhang, "Evolution mechanism of water-conducting channel of collapse column in karst mining area of Southwest China," *Geofluids*, vol. 2021, Article ID 6630462, 8 pages, 2021.

[6] W. L. Shen, J. B. Bai, W. F. Li, and X. Y. Wang, "Prediction of relative displacement for entry roof with weak plane under the effect of mining abutment stress," *Tunnelling and Underground Space Technology*, vol. 71, pp. 309–317, 2018.

[7] Y. Tian, H. Liu, X. Jiang, and R. Yu, "Analysis of stress and deformation of a positive buried pipe using the improved Spangler model," *Soils and Foundations*, vol. 55, no. 3, pp. 485–492, 2015.

[8] R. Khademi-Zahedi, "Application of the finite element method for evaluating the stress distribution in buried damaged polyethylene gas pipes," *Underground Space*, vol. 4, no. 1, pp. 59–71, 2019.

[9] H. G. Wu, J. H. Yu, C. Z. Shi, and Z. Ma, "Pipe-soil interaction and sensitivity study of large-diameter buried steel pipes," *KSCE Journal of Civil Engineering*, vol. 25, no. 3, pp. 793–804, 2021.

[10] Z. Wang, Z. Lu, D. Zhang, and H. Liu, "Stress effect of the interface between buried pipeline and sandy soil layer in a cold environment," *Cold Regions Science and Technology*, vol. 172, p. 102981, 2020.

[11] J. Zhang, Y. Chen, B. F. Liang, and B. Pan, "Damage evolution mechanism of buried pipeline crossing reverse fault," *Journal of Mechanical Science and Technology*, vol. 35, no. 1, pp. 71–77, 2021.

[12] S. Bildik and M. Laman, "Experimental investigation of soil-structure-pipe interaction," *KSCE Journal of Civil Engineering*, vol. 22, no. 9, pp. 3753–3763, 2019.

[13] D. W. Zhou, K. Wu, G. L. Cheng, and L. Li, "Mechanism of mining subsidence in coal mining area with thick alluvium soil in China," *Arabian Journal of Geosciences*, vol. 8, no. 4, pp. 1855–1867, 2015.

[14] Z. Joneidi, S. A. Mostafavi, and M. Motahari, "Simulation of buried natural gas pipelines and determination of optimum safe depth," *Journal of Failure Analysis and Prevention*, vol. 20, no. 5, pp. 1784–1793, 2020.

[15] M. Meidani, M. A. Meguid, and L. E. Chouinard, "Estimating earth loads on buried pipes under axial loading condition: insights from 3D discrete element analysis," *International Journal of Geo-Engineering*, vol. 9, no. 1, p. 5, 2018.

[16] J. Zhang, Y. Chen, and H. Zhang, "Local buckling evolution mechanism of a buried steel pipe under fault movements," *Energy science&Engineering*, vol. 8, no. 2, pp. 412–425, 2020.

[17] R. Liu and X. Y. Wang, "Lateral global buckling of submarine pipelines based on the model of nonlinear pipe–soil interaction," *China Ocean Engineering*, vol. 32, no. 3, pp. 312–322, 2018.

[18] K. Ono, K. Terada, Y. Sawada, H. I. Ling, and T. Kawabata, "Fluid coupled-DEM simulation of lateral loading experiment for buried pipe in saturated sand," *Transportation Infrastructure Geotechnology*, vol. 5, no. 2, pp. 93–113, 2018.

[19] D. Weerasinghe, J. Kodikara, and H. Bui, "Numerical modelling of swelling/shrinkage behaviour of unsaturated soils for buried pipe stress analysis," *Unsaturated Soil Mechanics from Theory to Practice-Proceedings of the 6th Asia-Pacific Conference on Unsaturated Soils*, pp. 615–620, 2015.

[20] A. Monshizadeh Naeen and E. Seyedi Hosseininia, "Numerical investigation on the deformational behavior of continuous buried pipelines under reverse faulting," *Arabian Journal for Science and Engineering*, vol. 45, no. 10, pp. 8475–8490, 2020.

[21] Y. F. ZOU, *Mining Subsidence Engineering*, China University of Mining and Technology Press, 2003.

[22] Y. Xue, P. G. Ranjith, F. Dang et al., "Analysis of deformation, permeability and energy evolution characteristics of coal mass around borehole after excavation," *Natural Resources Research*, vol. 29, no. 5, pp. 3159–3177, 2020.

[23] W. B. Guo and Q. Yong, "Study on the synergy acting model of high voltage power transmission lines tower, groundwork and foundation influenced by mining," *Journal of China Coal Society*, vol. 36, no. 7, pp. 1075–1080, 2011.

[24] Z. Z. Cao, P. Xu, Z. H. Li, M. X. Zhang, Y. Zhao, and W. L. Shen, "Joint bearing mechanism of coal pillar and backfilling body in roadway backfilling mining technology," *CMC-Computers Materials & Continua*, vol. 54, no. 2, pp. 137–159, 2018.

[25] X. Xu, K. He, and Y. Su, "Safety analysis of pipe–soil coordination deformation affected by mining subsidence," *Geotechnical and Geological Engineering*, vol. 38, no. 2, pp. 2187–2198, 2020.

[26] Y. Xue, T. Teng, F. Dang, Z. Ma, S. Wang, and H. Xue, "Productivity analysis of fractured wells in reservoir of hydrogen and carbon based on dual-porosity medium model,"

International Journal of Hydrogen Energy, vol. 45, no. 39, pp. 20240–20249, 2020.

[27] Y. D. J. Costa, J. G. Zornberg, and C. M. L. Costa, "Physical modeling of buried PVC pipes overlying localized ground subsidence," *Acta Geotechnica*, vol. 16, no. 3, pp. 807–825, 2020.

[28] Y. Xue, J. Liu, F. Dang, X. Liang, S. Wang, and Z. Ma, "Influence of CH_4 adsorption diffusion and CH_4-water two-phase flow on sealing efficiency of caprock in underground energy storage," *Sustainable Energy Technologies and Assessments*, vol. 42, article 100874, 2020.

[29] Y. Xue, F. Gao, Y. Gao, X. Liang, Z. Zhang, and Y. Xing, "Thermo-hydro-mechanical coupled mathematical model for controlling the pre-mining coal seam gas extraction with slotted boreholes," *International Journal of Mining Science and Technology*, vol. 27, no. 3, pp. 473–479, 2017.

[30] X. S. Zhe and A. Q. Gu, "Study on soil pressure of buried pipeline in gully terrain," *Journal of Xi'an Institute of Highway.*, vol. 7, no. 4, pp. 33–39, 1989.